# Sodium-Promoted Pd/TiO$_2$ for Catalytic Oxidation of Formaldehyde at Ambient Temperature

Changbin Zhang,[†] Yaobin Li,[†] Yafei Wang, and Hong He*

Research Center for Eco-Environmental Sciences, Chinese Academy of Sciences, Beijing 100085, China

Ⓢ *Supporting Information*

ABSTRACT: Catalytic oxidation of formaldehyde (HCHO) to CO$_2$ at ambient conditions is of great interest for indoor HCHO purification. Here, we report that sodium-doped Pd/TiO$_2$ is a highly effective catalyst for the catalytic oxidation of HCHO at room temperature. It was observed that Na doping has a dramatic promotion effect on the Pd/TiO$_2$ catalyst and that nearly 100% HCHO conversion could be achieved over the 2Na−Pd/TiO$_2$ catalyst at a GHSV of 95000 h^{-1} and HCHO inlet concentration of 140 ppm at 25 °C. The mechanism of the Na-promotion effect was investigated by using Brunauer−Emmett−Teller (BET), X-ray diffraction (XRD), CO chemisorption, Temperature-programmed reduction by H$_2$ (H$_2$-TPR), X-ray photoelectron spectroscopy (XPS) and temperature-programmed desorption of O$_2$ (O$_2$-TPD) methods. The results showed that Na species addition can induce and further stabilize a negatively charged and well-dispersed Pd species, which then facilitates the activation of H$_2$O and chemisorbed oxygen, therefore resulting in the high performance of the 2Na−Pd/TiO$_2$ catalyst for the ambient HCHO destruction.
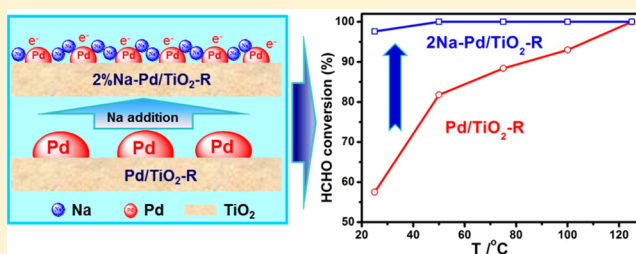
INTRODUCTION

The "sick building syndrome" has become a critical issue in most new houses as a result of increasing concerns about indoor air pollutants.[1] Formaldehyde (HCHO) emitted from building/furnishing materials and consumer products is recognized as a major indoor air pollutant in airtight houses and is known to cause nasal tumors, irritation of the mucous membranes of the eyes and respiratory tract, and skin irritation.[2,3] Therefore, in order to improve indoor air quality and reduce public health risk, the effective abatement of indoor air HCHO is urgently needed.

Over the past decades, researchers have focused on four technologies for the removal of HCHO: adsorption, photocatalysis, plasma technology, and catalytic oxidation.[4−9] The adsorption is a useful method for indoor air HCHO removal. Some absorbents can successfully reduce indoor HCHO concentrations to very low levels;[4] however, their effectiveness is limited by adsorption capacities and the secondary pollution during regeneration. The catalytic oxidation method can selectively decompose the low concentration toxic HCHO to harmless CO$_2$ over some catalysts at ambient temperature without the need of energy input.[9,10] Therefore, the catalytic oxidation is regarded as the most promising method for indoor air HCHO removal.[9,10]

The conventional catalysts for HCHO oxidation include transition-metal oxides (Ni, Co, Ag, and Mn)[11−17] and the supported noble metal (Pt, Pd, Rh, and Au) catalysts.[18−28] The transition-metal oxides generally need much high temperatures (>150 °C) to achieve complete oxidation of HCHO. In contrast, the noble metal catalysts such as Pt-, Pd-, and Au-based catalysts have exhibited excellent activity for catalytic oxidation of HCHO at around 25 °C[18,20−23,26−28] and, therefore, are more suitable for indoor air HCHO purification.

Previuosly, we have developed a Pt/TiO$_2$ catalyst for HCHO catalytic oxidation, achieving 100% conversion of 100 ppm of HCHO to CO$_2$ and H$_2$O at a gas hourly space velocity (GHSV) of 50000 h^{-1} at room temperature.[20−22] Then, we further demonstrated that the addition of alkali ions (such as Li$^+$, Na$^+$, and K$^+$) could dramatically promote the catalytic efficacy of Pt/TiO$_2$ catalyst by inducing and stabilizing an atomically dispersed Pt species.[26] We also proposed that this promotion effect of alkali ions on Pt catalysts may apply to other noble-metal-based catalysts.[26] Instead of Pt-based catalysts, Pd-based catalysts are much less expensive and will have more extensive application for indoor air HCHO purification. Therefore, it is worth exploring whether the Na-promotion effect for Pt is also manifested for Pd catalysts.

In this paper, we prepared Pd/TiO$_2$ catalysts with and without sodium (Na) addition and tested their catalytic activities in HCHO oxidation at low temperature. It was verified that the Na addition also had a dramatic promotion effect on the Pd-based catalyst. Na−Pd/TiO$_2$ (2 wt %) showed much higher performance in ambient HCHO oxidation than the Na-free catalyst, achieving 100% conversion of 140 ppm of HCHO to CO$_2$ and H$_2$O at a gas hourly space velocity

Table 1. Bulk Composition, Specific Surface Area (BET), Average Pore Size (d), and Total Pore Volume (V) of Pd/TiO₂ and 2Na−Pd/TiO₂ Catalysts together with TiO₂, and Pd Dispersion (D) and Metal Size on Pd/TiO₂-R and 2Na−Pd/TiO₂-R catalysts

sample	bulk comp^a (wt %)		BET (m^2/g)	d_p (nm)	V (cm^3/g)	$D_{co}{}^b$ (%)	metal size^c d_m (nm)
	Pd	Na					
TiO₂			58.9	28.2	0.43		
Pd/TiO₂	0.99		56.5	28.1	0.40		
Pd/TiO₂-R			53.1	28.7	0.38	9.8	11.4
2Na−Pd/TiO₂	0.95	1.95	46.5	31.7	0.37		
2Na−Pd/TiO₂-R			56.9	26.8	0.38	32.9	3.4

^{a}Bulk composition was measured by ICP-OES. ^{b}Dispersion of Pd measured by CO chemisorption. $^c d_m$ (Å) = 11.2/D_{co}.[30]

(GHSV) of 95 000 h^{-1} at 25 °C. Based on the characterization results, the mechanism of Na-promotion effect on the Pd/TiO₂ catalyst was clearly elucidated.

■ EXPERIMENTAL SECTION

Materials Preparation. The 1 wt % Pd/TiO₂, 2 wt % Na/TiO₂, and 2 wt % Na−1 wt % Pd/TiO₂ samples were prepared by co-impregnation of TiO₂ (Degussa P25, BET surface area 59 m^{2}g^{-1}) with aqueous NaNO₃ and Pd(NO₃)₂ (Aldrich) for 1 h. After impregnation, the excess water was removed in a rotary evaporator at 60 °C. The samples were dried at 110 °C for 12 h and then calcined at 400 °C for 2 h. The samples reduced with H₂ at 350 °C for 30 min were denoted as 2Na/TiO₂-R, Pd/TiO₂-R, and 2Na−Pd/TiO₂-R. The actual Pd and Na loading amounts in Pd/TiO₂ and 2Na−Pd/TiO₂ were measured using inductively coupled plasma optical emission spectrometry (ICP-OES) (OPTIMA 8300, PerkinElmer), and the data are presented in Table 1.

Material Characterization. X-ray powder diffraction (XRD) patterns of the catalyst samples were collected with an X'Pert PRO MPD X-ray powder diffractometer with Cu Kα radiation operated at 40 kV and 40 mA. The patterns were measured over the 2θ range from 10° to 90° at a scan step of 0.02°. The specific surface area and pore characterization of the catalysts was obtained at −196 °C over the whole range of relative pressures, using a Quantachrome Quadrasorb SI-MP analyzer. Prior to the N₂ physisorption, the catalysts were degassed at 300 °C for 5 h. Specific surface areas were calculated from the isotherms by applying the BET equation in the 0.05−0.3 partial pressure range.

CO chemisorption, H₂ temperature-programmed reduction (H₂-TPR), and O₂ temperature-programmed desorption (O₂-TPD) were performed in a Micromeritics AutoChem II 2920 apparatus, equipped with a computer-controlled CryoCooler and a thermal conductivity detector (TCD).

CO chemisorption was measured by a dynamic pulse method.[28] The samples (30 mg, 40−60 mesh) were reduced at 350 °C for 30 min in 10% H₂/Ar (50 mL min^{-1}), followed by flushing in He (50 mL min^{-1}) for 30 min. Then, the temperature was lowered to room temperature in He flow. Pulses of 5% CO/He were introduced to the catalyst until uptake saturation was obtained. The CO consumption was monitored by TCD. The dispersion of Pd was calculated assuming a CO/Pd stoichiometric ratio of 1.[27,29] The crystallite sizes of the dispersed metals were estimated from the CO chemisorption data, using the relation d_M (Å) = 11.2/D_{co},[30] where d_M is the mean crystallite diameter and D_{co} is the dispersion of the metals.

For H₂-TPR, reduction profiles were obtained by passing a flow of 10% H₂/Ar at a rate of 50 mL min^{-1} (STP) through the sample (weight around 60 mg). The temperature was increased from −50 to +450 °C at a rate of 10 °C min^{-1}, and the H₂ consumption was monitored by TCD after removal of produced H₂O.

For O₂-TPD, the samples were first prereduced with 10% H₂/Ar at 350 °C for 30 min, followed by purging with He for 30 min to desorb H₂. The temperature was then cooled down to 25 °C, and then the gas was switched to O₂ for adsorption for 30 min. After that, He flowed for 1 h to remove weakly adsorbed O₂. The temperature was increased to 400 °C at a heating rate of 10 °C min^{-1}.

X-ray photoelectron spectra (XPS) were measured by an AXIS Ultra system, equipped with Al Kα radiation ($h\nu$ = 1486.6 eV) with an X-ray anode operated at 225 W and 15 kV. The C 1s peak (284.8 eV) was used to calibrate the binding energy (BE) values. The surface relative composition was estimated from the integrated intensities corrected by atomic sensitivity factors.

Activity Test for Formaldehyde Oxidation. The activity tests for the catalytic oxidation of HCHO over the catalysts (60 mg) were performed in a fixed-bed quartz flow reactor (i.d. = 4 mm) in an incubator where the temperature was kept at 25 °C. Gaseous HCHO was generated by flowing helium through the paraformaldehyde container in a water bath kept at 35 °C. Water vapor was generated by flowing helium through a water bubbler at 25 °C. The feed gas composition is 140 ppm of HCHO, 20% O₂ and 25% RH balanced by helium. The total flow rate was 100 mL min^{-1}, corresponding to a gas hourly space velocity (GHSV) of 95 000 h^{-1}. The inlet and outlet gases were monitored by FTIR (Nicolet 380) equipped with 2 m gas cell and a DTGS detector; resolution: 0.5 cm^{-1}; OPD velocity: 0.4747 cm s^{-1}. The collect region was 4000−600 cm^{-1} and the number of scans per spectrum was 16 times. The representative FTIR spectra for HCHO oxidation reactions over 2Na−Pd/TiO₂-R are shown in Figure S1 (Supporting Information). HCHO and CO₂ were measured by the peaks located at 2897 (C−H vibration) and 2350 cm^{-1} (O−C−O vibration), respectively. Since no other carbon-containing compounds except for CO₂ were detected in the effluents for all tested catalysts, the HCHO and CO₂ concentrations were quantified and calculated based on the peak area of CO₂ at 2350 cm^{-1}. Before the measurement, a CO₂ standard curve was created using the different CO₂ concentrations vs the peak areas at 2350 cm^{-1} and shown in Figure S2 (Supporting Information). The standard curve showed that the CO₂ concentration below 500 ppm is a linear function of the peak area at 2350 cm^{-1}.

■ RESULTS AND DISCUSSION

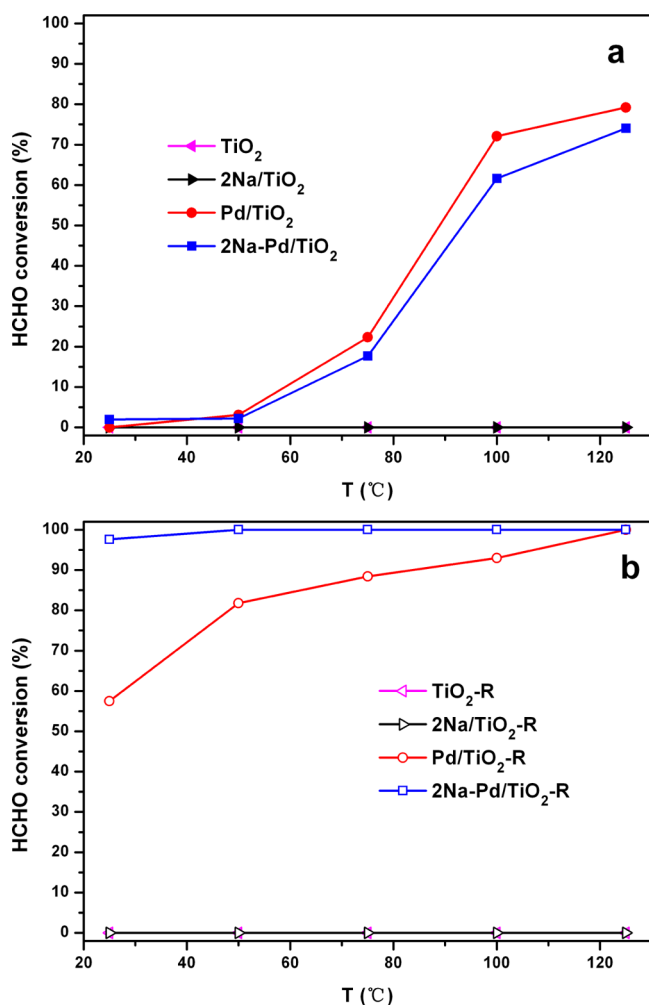**Activity Test.** Figure 1 shows the HCHO conversion over Pd/TiO$_2$ and 2Na−Pd/TiO$_2$ catalysts together with pure TiO$_2$

Figure 1. HCHO conversion over TiO$_2$, 2Na/TiO$_2$, Pd/TiO$_2$, and 2Na−Pd/TiO$_2$ samples before (a) and after (b) reduction at different temperatures. Reaction conditions: 140 ppm of HCHO, 20% O$_2$, 25% RH, He balance, GHSV 95 000 h^{-1}.

and 2Na/TiO$_2$ before (a) and after (b) pretreatment by H$_2$. Pure TiO$_2$ and 2Na/TiO$_2$ had no activity for HCHO oxidation at low temperatures (25−125 °C) whether or not H$_2$ reduction occurred. 2Na−Pd/TiO$_2$ catalyst showed a similar activity to Na-free catalyst before H$_2$ pretreatment, but both of them were not active for HCHO oxidation at ambient temperatures (Figure 1a). In contrast, after H$_2$ reduction, the activities of both Pd/TiO$_2$ and Na−Pd/TiO$_2$ catalysts were greatly enhanced in the low temperature range (Figure 1b), indicating that metallic Pd species are active sites for the low temperature oxidation of HCHO. Remarkably, Na addition demonstrated a dramatic promotion effect on the reduced Pd/TiO$_2$. The Pd/TiO$_2$-R catalyst only presented about 55% HCHO conversion, while the 2Na−Pd/TiO$_2$-R catalyst achieved almost 100% conversion of 140 ppm of HCHO at a GHSV of 95 000 h^{-1} at 25 °C. The catalytic performance of the 2Na−Pd/TiO$_2$-R catalyst was also checked by long isothermal tests at 25 °C. As shown in Figure 2, the sample exhibited excellent stability and

efficiency with the same reaction conditions, and approximately 100% HCHO conversion was maintained over a 30 h long test.
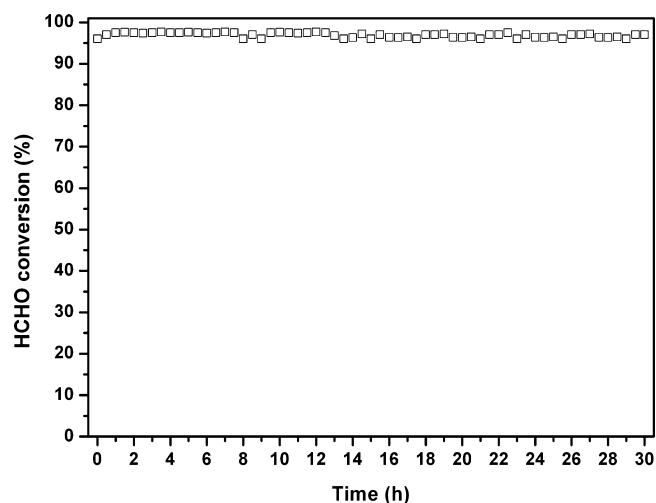

Figure 2. Stability test of 2Na−Pd/TiO$_2$-R. Reaction conditions: 25 °C, 140 ppm of HCHO, 20% O$_2$, 25% RH, He balance, GHSV 95000 h^{-1}.

Structural Features of Catalysts. XRD patterns of Pd/TiO$_2$ and 2Na−Pd/TiO$_2$ catalysts before and after H$_2$ pretreatment together with TiO$_2$ are shown in Figure 3. No
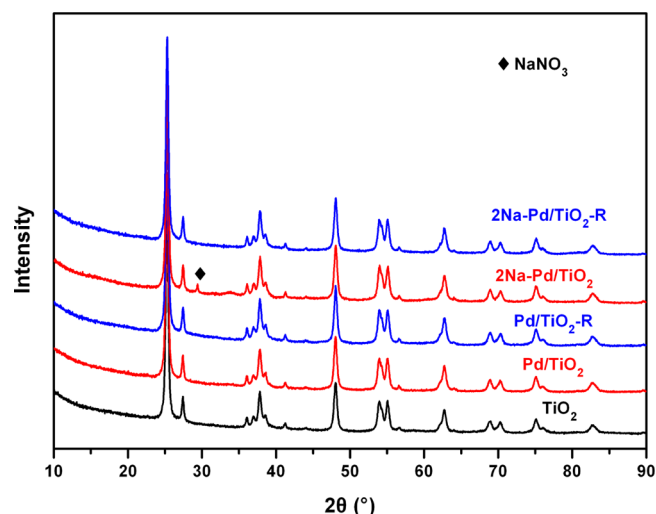

Figure 3. XRD patterns of Pd/TiO$_2$, 2Na−Pd/TiO$_2$, Pd/TiO$_2$-R, and 2Na−Pd/TiO$_2$-R together with TiO$_2$ samples.

Pd species (Pd^0, PdO) were observed in any samples, indicating that Pd species are highly dispersed on the TiO$_2$ support. On the 2Na−Pd/TiO$_2$ catalyst, a residual diffraction peak from undecomposed NaNO$_3$ (PDF No. 00-001-0840) was observed at 2Θ = 29.4°, and it disappeared after H$_2$ treatment at 350 °C, implying that the residual NaNO$_3$ was reduced.[31]

The specific surface area (S_{BET}), average pore size (d), and total pore volume (V) of Pd/TiO$_2$ and 2Na−Pd/TiO$_2$ catalysts before and after H$_2$ pretreatment were next measured, the results are listed in Table 1, and the plots of pore size distribution are shown in Figure S3 (Supporting Information). The Pd/TiO$_2$ catalyst showed a similar S_{BET}, V, and average pore size (d) to bare TiO$_2$ whether or not H$_2$ reduction had

taken place. The Na addition to Pd/TiO$_2$ catalyst decreased the S_{BET} and V but increased the average pore size (d), probably due to the deposition of NaNO$_3$ inside the small pores of TiO$_2$. During the H$_2$ reduction at 350 °C, some Na species possibly migrated out of the small pores, increasing the S_{BET} and V and decreasing the average pore size (d) of the 2Na−Pd/TiO$_2$-R sample.

Pd Dispersion and Sizes on Catalysts. Pd dispersion was determined by CO chemisorption, and Pd particle sizes were calculated based on Pd dispersion degree. The results of Pd dispersion and particle size are shown in Table 1. Without Na addition, the Pd dispersion was only 9.8% and the Pd particle size was around 11.4 nm on the Pd/TiO$_2$-R catalyst. Na addition to Pd/TiO$_2$ remarkably increased the Pd dispersion to 32.9%, and the Pd particle size sharply dropped to 3.4 nm. Clearly, Na addition induces a more dispersed Pd species on 2Na−Pd/TiO$_2$-R catalyst that exposes more Pd sites for HCHO oxidation, therefore significantly promoting the activity of the Pd/TiO$_2$ catalyst.

Reducibility of Catalysts. H$_2$-TPR was conducted to study the reducibility of the catalysts, and the TPR profiles of Pd/TiO$_2$, 2Na−Pd/TiO$_2$, 2Na/TiO$_2$, and pure TiO$_2$ are shown in Figure 4. Pure TiO$_2$ exhibited no H$_2$ consumption peak in the
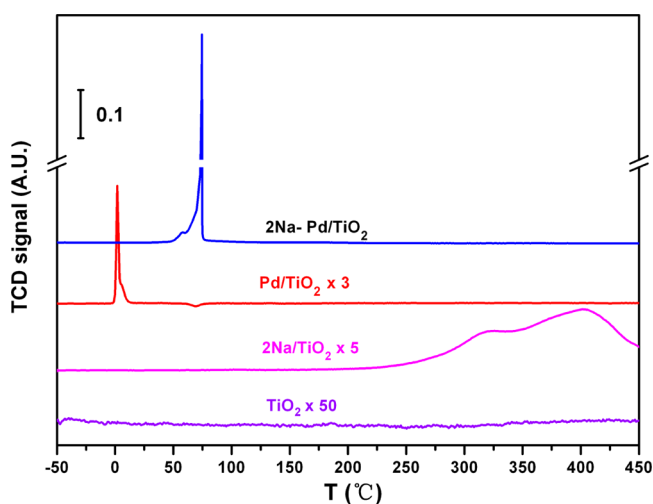

Figure 4. H$_2$-TPR profiles of TiO$_2$, 2Na/TiO$_2$, Pd/TiO$_2$, and 2Na−Pd/TiO$_2$ samples.

−50 to +450 °C range since TiO$_2$ reduction normally occurs at $T > 600$ °C.[32] The 2Na/TiO$_2$ sample presented a broad peak at 200−450 °C, which is assigned to the reduction of Na species.[31] After Pd was loaded, Pd/TiO$_2$ showed a sharp PdO reduction peak at around 0 °C.[33] With the further addition of Na, the PdO reduction peak shifted to higher temperature at about 58 °C, while the reduction peak of Na species shifted toward low temperature, at about 75 °C. The above results indicate a strong interaction between the Na species and Pd species, with the Na species stabilizing the Pd species and the existence of Pd species facilitating the reduction of the Na species.[31,34]

XPS Analysis. XPS measurements were next carried out to identify the states of Pd, Ti O and Na elements on the catalyst surface. The XPS spectra are shown in Figure 5; the binding energies and the percentages of XPS peaks calculated are summarized in Table 2. As shown in Figure 5a, the fresh Pd/TiO$_2$ and 2Na−Pd/TiO$_2$ only presented one Pd 3d$_{5/2}$ peak

centered at 336.4 eV, indicating that the Pd species are all in the oxide state.[35] After the catalysts were reduced at 350 °C, Pd/TiO$_2$-R displayed two Pd 3d$_{5/2}$ peaks at 336.4 and 335.1 eV characteristic of Pd oxide and metallic Pd. The calculation results (Table 2) showed that about 66% of Pd species were in the metallic Pd state. In contrast, with Na addition, the 2Na−Pd/TiO$_2$-R catalyst presented a third Pd 3d$_{5/2}$ peak at the low binding energy of 334.0 eV alongside the peaks at 336.4 and 335.1 eV, indicating that the doped Na, as an electron donor, leads to the formation of a negatively charged Pd species by its strong interaction with metallic Pd.[36,37] This formed negatively charged Pd species could enhance O$_2$ adsorption by the donation of electrons from Pd metal to the antibonding π^* orbital of O$_2$.[27,38] In addition, it was dominant (65.1%) on the 2Na−Pd/TiO$_2$-R catalyst surface, therefore playing the key role in the ambient HCHO oxidation.

Figure 5b shows the Ti 2p peaks of the series of catalysts. The peak at 458.8 eV over the Pd/TiO$_2$ catalyst was ascribed to Ti^{4+} of TiO$_2$.[27] A slight negative shift of 0.3 eV over Pd/TiO$_2$-R should be related to the formation of TiO$_{2-x}$ species during the reduction process.[39] In comparison, after Na addition, the Ti 2p peaks shifted to 458.3 eV over 2Na−Pd/TiO$_2$ and 2Na/TiO$_2$ and then shifted to 458.0 eV over 2Na−Pd/TiO$_2$-R and 2Na/TiO$_2$-R samples. The above findings show that the doped Na species may interact with the support and improve the reduction of TiO$_2$.[40] This finding is consistent with the observations of Onishi, et al.,[41] who reported that Na deposited on TiO$_2$ (110) strongly interacted with surface oxygen atoms thereby causing the charge transfer to the substrate and the reduction of Ti^{4+} to Ti^{3+}.

Figure 5c shows the O 1s XPS spectra of the catalysts. Two kinds of O species were observed in all samples. The main peak at the binding energy range of 529.2−529.7 eV was assigned to the lattice oxygen of bulk TiO$_2$ (O$_I$), and the small shoulder peak at the binding energy range 530.8−531.5 eV was ascribed to Ti−OH.[39] As can be seen in Table 2, the percentage of Ti−OH species (O$_{II}$) was about 9.0% over the Pd/TiO$_2$-R samples, while the percentage of Ti−OH species (O$_{II}$) increased to 15.7% over the 2Na−Pd/TiO$_2$-R catalyst, demonstrating that Na addition increases the concentration of surface OH groups.[42] We have reported that the reaction between surface OH and formate species to give final products is a facile reaction pathway for ambient HCHO oxidation.[26] Therefore, in this work, the enhancement of surface OH concentration with Na addition also partially accounts for the activity improvement of 2Na−Pd/TiO$_2$-R.

The XPS data of Na 1s are shown in Figure 5d. Peaks at 1071.3 eV over 2Na/TiO$_2$ and 2Na−Pd/TiO$_2$ catalysts were ascribed to Na$^+$ in the form of NaNO$_3$,[43] further confirming the successful loading of Na species on TiO$_2$. After the catalysts were reduced, the Na 1s peaks were shifted to lower band energy, which could be attributed to the partial reduction of surface Na$^+$ or the incorporation of Na$^+$ into TiO$_2$.[44]

O$_2$-TPD. O$_2$-TPD experiments were next performed to investigate the O$_2$ activation over the Pd/TiO$_2$-R and 2Na−Pd/TiO$_2$-R catalysts, and the profiles are shown in Figure 6. There was only one broad O$_2$ desorption peak presented on both Pd/TiO$_2$-R and 2Na−Pd/TiO$_2$-R samples in the temperature range of 25 to 400 °C. For the Pd/TiO$_2$-R catalyst, the O$_2$ desorption occurred at 142 °C and the peak was centered at 221 °C. After Na addition, the O$_2$ desorption peak shifted to the low temperature range, starting at 89 °C and centered at 180 °C, indicating that Na species addition enhanced the mobility and
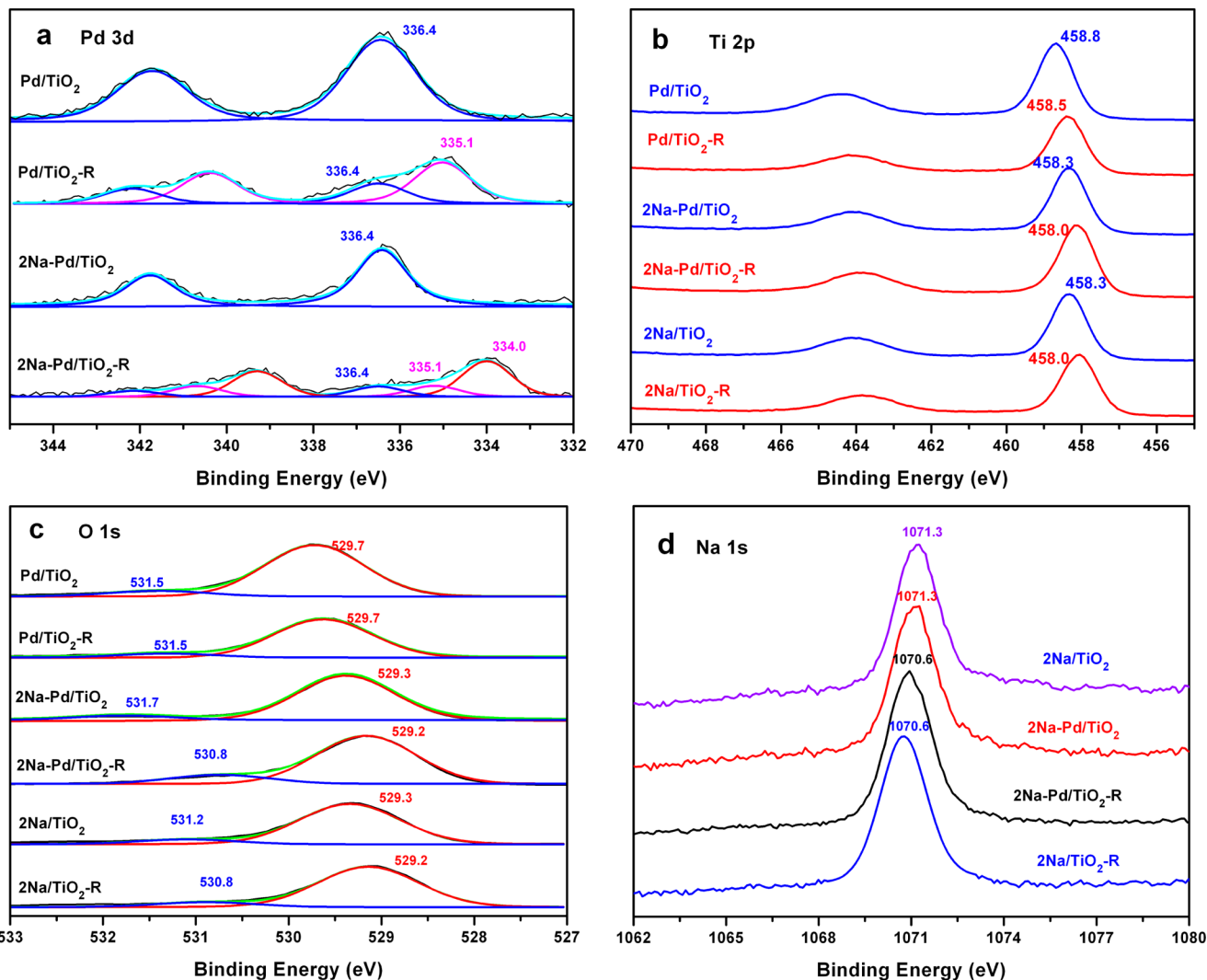
Figure 5. XPS spectra of Pd/TiO$_2$, 2Na−Pd/TiO$_2$, Pd/TiO$_2$-R, and 2Na−Pd/TiO$_2$-R together with 2Na/TiO$_2$ and 2Na/TiO$_2$-R samples: (a) Pd 3d, (b) Ti 2p, (c) O 1s, and (d) Na 1s.

Table 2. XPS Data of Pd/TiO$_2$, 2Na−Pd/TiO$_2$, Pd/TiO$_2$-R and 2Na−Pd/TiO$_2$-R together with 2Na/TiO$_2$ and 2Na/TiO$_2$-R Samples

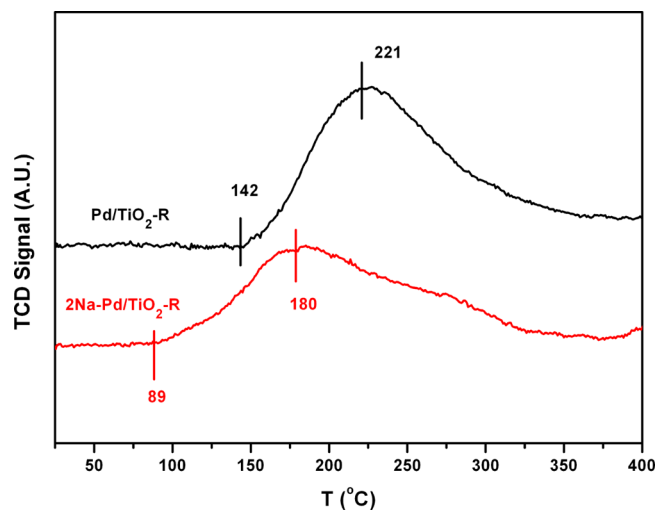| samples	Pd 3d B.E. (eV)	ratio (%)	O 1s B.E. (eV)	ratio (%)	Ti 2p B.E. (eV)	Na 1s B.E. (eV)
Pd/TiO$_2$	336.4		529.7	91.1	458.8	
			531.4	8.9		
Pd/TiO$_2$-R	335.1	66.0	529.1	90.5	458.5	
	336.4	34.0	531.4	9.5		
2Na−Pd/TiO$_2$	336.4		529.3	91.1	458.3	1071.3
			531.8	8.9		
2Na−Pd/TiO$_2$-R	334.0	65.1	529.2	84.3	458.0	1070.6
	335.1	19.3	530.8	15.7		
	336.4	15.6				
2Na/TiO$_2$			529.3	91.0	458.3	1071.3
			531.2	9.0		
2Na/TiO$_2$-R			529.2	89.1	458.0	1070.6
			530.8	10.9		

Figure 6. O$_2$−TPD profiles of Pd/TiO$_2$-R and 2Na−Pd/TiO$_2$-R samples.

activation of the chemisorbed oxygen over the 2Na−Pd/TiO$_2$-R catalyst. The enhanced activation of chemisorbed oxygen by

Na addition should also contribute to the excellent activity of 2Na−Pd/TiO$_2$-R.

In summary, this work demonstrates that the Na addition has a dramatic promotion effect on this Pd-based catalyst for ambient HCHO oxidation. As shown above, Na addition to Pd/TiO_2 led to the formation of a well-dispersed Pd species that facilitated the activation of surface OH groups and chemisorbed oxygen and thus significantly increased the catalytic activity of Pd/TiO_2 catalyst for ambient HCHO destruction. This work further confirmed the alkali ion promotion effect on the catalytic activity of noble metal based catalysts.

■ ASSOCIATED CONTENT

Ⓢ Supporting Information

Representative FTIR spectra for HCHO oxidation reactions, the standard curve of CO_2 concentration, and plots of pore size distribution. This material is available free of charge via the Internet at http://pubs.acs.org/.

■ AUTHOR INFORMATION

Corresponding Author

*Phone: 86-10-62849123. Fax: 86-10-62849123. E-mail: honghe@rcees.ac.cn.

Author Contributions

[†]These authors contributed equally to this work.

Notes

The authors declare no competing financial interest.

■ ACKNOWLEDGMENTS

■ REFERENCES

(1) Yu, C.; Crump, D. A review of the emission of VOCs from polymeric materials used in buildings. *Build. Environ.* **1998**, *33* (6), 357–374.

(2) Maddalena, R.; Russell, M.; Sullivan, D. P.; Apte, M. G. Formaldehyde and Other Volatile Organic Chemical Emissions in Four FEMA Temporary Housing Units. *Environ. Sci. Technol.* **2009**, *43* (15), 5626–5632.

(3) Formaldehyde: Assessing the risk. *Environ. Sci. Technol.* **1984**, *18*, (7), 216A–221A.

(4) Rong, H.; Liu, Z.; Wu, Q.; Pan, D.; Zheng, J. Formaldehyde removal by Rayon-based activated carbon fibers modified by P-aminobenzoic acid. *Cellulose* **2009**, *17* (1), 205–214.

(5) Moreno-Pirajan, J. C.; Tirano, J.; Salamanca, B.; Giraldo, L. Activated carbon modified with copper for adsorption of propanethiol. *Int. J. Mol. Sci.* **2010**, *11* (3), 927–942.

(6) Noguchi, T.; Fujishima, A.; Sawunyama, P.; Hashimoto, K. Photocatalytic Degradation of Gaseous Formaldehyde Using TiO_2 Film. *Environ. Sci. Technol.* **1998**, *32* (23), 3831–3833.

(7) Shiraishi, F.; Ohkubo, D.; Toyoda, K.; Yamaguchi, S. Decomposition of gaseous formaldehyde in a photocatalytic reactor with a parallel array of light sources. *Chem. Eng. J.* **2005**, *114* (1–3), 153–159.

(8) Chang, M. B.; Lee, C. C. Destruction of formaldehyde with dielectric barrier discharge plasmas. *Environ. Sci. Technol.* **1995**, *29* (1), 181–186.

(9) Quiroz Torres, J.; Royer, S.; Bellat, J. P.; Giraudon, J. M.; Lamonier, J. F. Formaldehyde: catalytic oxidation as a promising soft way of elimination. *ChemSusChem* **2013**, *6* (4), 578–592.

(10) Pei, J.; Zhang, J. S. Critical review of catalytic oxidization and chemisorption methods for indoor formaldehyde removal. *HVAC&R Res.* **2011**, *17* (4), 476–503.

(11) Bai, B. Y.; Arandiyan, H.; Li, J. H. Comparison of the performance for oxidation of formaldehyde on nano-Co_3O_4, 2D-Co_3O_4, and 3D-Co_3O_4 catalysts. *Appl. Catal. B* **2013**, *142*, 677–683.

(12) Ma, L.; Wang, D.; Li, J.; Bai, B.; Fu, L.; Li, Y. Ag/CeO_2 nanospheres: Efficient catalysts for formaldehyde oxidation. *Appl. Catal., B* **2014**, *148–149*, 36–43.

(13) Qu, Z.; Shen, S.; Chen, D.; Wang, Y. Highly active Ag/SBA-15 catalyst using post-grafting method for formaldehyde oxidation. *J. Mol. Catal. A: Chem.* **2012**, *356*, 171–177.

(14) Imamura, S.; Uchihori, D.; Utani, K.; Ito, T. Oxidative Decomposition of Formaldehyde on Silver-Cerium Composite Oxide Catalyst. *Catal. Lett.* **1994**, *24* (3–4), 377–384.

(15) Wen, Y.; Tang, X.; Li, J.; Hao, J.; Wei, L.; Tang, X. Impact of synthesis method on catalytic performance of MnO_x–SnO_2 for controlling formaldehyde emission. *Catal. Commun.* **2009**, *10* (8), 1157–1160.

(16) Chen, T.; Dou, H.; Li, X.; Tang, X.; Li, J.; Hao, J. Tunnel structure effect of manganese oxides in complete oxidation of formaldehyde. *Micropor. Mesopor. Mater.* **2009**, *122* (1–3), 270–274.

(17) Tang, X.; Li, Y.; Huang, X.; Xu, Y.; Zhu, H.; Wang, J.; Shen, W. MnO_x–CeO_2 mixed oxide catalysts for complete oxidation of formaldehyde: Effect of preparation method and calcination temperature. *Appl. Catal., B* **2006**, *62* (3–4), 265–273.

(18) Xu, Q. J.; Zhang, Y. P.; Mo, J. H.; Li, X. X. Indoor Formaldehyde Removal by Thermal Catalyst: Kinetic Characteristics, Key Parameters, and Temperature Influence. *Environ. Sci. Technol.* **2011**, *45* (13), 5754–5760.

(19) Sekine, Y. Oxidative decomposition of formaldehyde by metal oxides at room temperature. *Atmos. Environ.* **2002**, *36* (35), 5543–5547.

(20) Zhang, C.; He, H.; Tanaka, K.-i. Perfect catalytic oxidation of formaldehyde over a Pt/TiO_2 catalyst at room temperature. *Catal. Commun.* **2005**, *6* (3), 211–214.

(21) Zhang, C.; He, H.; Tanaka, K.-i. Catalytic performance and mechanism of a Pt/TiO_2 catalyst for the oxidation of formaldehyde at room temperature. *Appl. Catal., B* **2006**, *65* (1–2), 37–43.

(22) Zhang, C.; He, H. A comparative study of TiO_2 supported noble metal catalysts for the oxidation of formaldehyde at room temperature. *Catal. Today* **2007**, *126* (3–4), 345–350.

(23) Kim, S. S.; Park, K. H.; Hong, S. C. A study on HCHO oxidation characteristics at room temperature using a Pt/TiO_2 catalyst. *Appl. Catal., A* **2011**, *398* (1–2), 96–103.

(24) Imamura, S.; Uematsu, Y.; Utani, K.; Ito, T. Combustion of formaldehyde on ruthenium/cerium (IV) oxide catalyst. *Ind. Eng. Chem. Res.* **1991**, *30* (1), 18–21.

(25) Álvarez-Galván, M. C.; de la Peña O'Shea, V. A.; Fierro, J. L. G.; Arias, P. L. Alumina-supported manganese- and manganese–palladium oxide catalysts for VOCs combustion. *Catal. Commun.* **2003**, *4* (5), 223–228.

(26) Zhang, C.; Liu, F.; Zhai, Y.; Ariga, H.; Yi, N.; Liu, Y.; Asakura, K.; Flytzani-Stephanopoulos, M.; He, H. Alkali-metal-promoted Pt/TiO_2 opens a more efficient pathway to formaldehyde oxidation at ambient temperatures. *Angew. Chem., Int. Ed.* **2012**, *51* (38), 9628–9632.

(27) Huang, H.; Leung, D. Y. C. Complete oxidation of formaldehyde at room temperature using TiO_2-supported metallic Pd nanoparticles. *ACS Catal.* **2011**, *1* (4), 348–354.

(28) Li, H.-F.; Zhang, N.; Chen, P.; Luo, M.-F.; Lu, J.-Q. High surface area Au/CeO_2 catalysts for low temperature formaldehyde oxidation. *Appl. Catal., B* **2011**, *110*, 279–285.

(29) Fox, E. B.; Velu, S.; Engelhard, M. H.; Chin, Y.-H.; Miller, J. T.; Kropf, J.; Song, C. Characterization of CeO_2-supported Cu–Pd bimetallic catalyst for the oxygen-assisted water–gas shift reaction. *J. Catal.* **2008**, *260* (2), 358–370.

(30) Anderson, J. R. *Structure of Metallic Catalysts*; Academic Press: London, 1975; Vol. 379.

(31) Zhu, X.; Shen, M.; Lobban, L. L.; Mallinson, R. G. Structural effects of Na promotion for high water gas shift activity on Pt–Na/TiO_2. *J. Catal.* **2011**, *278* (1), 123–132.

(32) de Resende, N. S.; Eon, J.-G.; Schmal, M. Pt/TiO$_2$−γ-Al$_2$O$_3$ catalyst: I. Dispersion of platinum on alumina-grafted titanium oxide. *J. Catal.* **1999**, *183* (1), 6−13.

(33) Zhu, H. Pd/CeO$_2$−TiO$_2$ catalyst for CO oxidation at low temperature: a TPR study with H$_2$ and CO as reducing agents. *J. Catal.* **2004**, *225* (2), 267−277.

(34) Gusovius, A. F.; Watling, T. C.; Prins, R. Ca promoted Pd/SiO$_2$ catalysts for the synthesis of methanol from CO: the location of the promoter. *Appl. Catal., A* **1999**, *188* (1−2), 187−199.

(35) Otto, K.; Haack, L. P.; deVries, J. E. Identification of two types of oxidized palladium on γ-alumina by X-ray photoelectron spectroscopy. *Appl. Catal., B* **1992**, *1* (1), 1−12.

(36) Liotta, L. F.; Deganello, G.; Delichere, P.; Leclercq, C.; Martin, G. A. Localization of alkali metal ions in sodium-promoted palladium catalysts as studied by low energy ion scattering and transmission electron microscopy. *J. Catal.* **1996**, *164* (2), 334−340.

(37) Liotta, L. F.; Martin, G. A.; Deganello, G. The influence of alkali metal ions in the chemisorption of CO and CO$_2$ on supported palladium catalysts: A fourier transform infrared spectroscopic study. *J. Catal.* **1996**, *164* (2), 322−333.

(38) Vayenas, C. G.; Bebelis, S; Pliangos, C.; Brosda, S.; Tsiplakides, D. *Electrochemical Activation of Catalysis: Promotion, Electrochemical Promotion, And Metal-Support Interactions*; Kluwer Academic Publishers/Plenum Press: New York, 2001.

(39) Nie, L.; Yu, J.; Li, X.; Cheng, B.; Liu, G.; Jaroniec, M. Enhanced performance of NaOH-modified Pt/TiO$_2$ toward room temperature selective oxidation of formaldehyde. *Environ. Sci. Technol.* **2013**, *47* (6), 2777−2783.

(40) Panagiotopoulou, P.; Kondarides, D. I. Effects of alkali promotion of TiO$_2$ on the chemisorptive properties and water−gas shift activity of supported noble metal catalysts. *J. Catal.* **2009**, *267* (1), 57−66.

(41) Onishi, H.; Aruga, T.; Egawa, C.; Iwasawa, Y. Modification of surface electronic-structure on TiO$_2$ (110) and TiO$_2$ (441) by Na deposition. *Surf. Sci.* **1988**, *199* (1−2), 54−66.

(42) Brookes, I.; Muryn, C.; Thornton, G. Imaging water dissociation on TiO$_2$ (110). *Phys. Rev. Lett.* **2001**, *87* (26), 266103(1−4).

(43) Wagner, C. D. Chemical shifts of Auger lines, and the Auger parameter. *Faraday Discuss. Chem. Soc.* **1975**, *60*, 291−300.

(44) Yoshida, A.; Shen, W.; Eda, T.; Watanabe, R.; Ito, T.; Naito, S. NOx storage/reduction over alkali-metal-nitrate impregnated titanate nanobelt catalysts and investigation of alkali metal cation migration using XPS. *Catal. Today* **2012**, *184* (1), 78−82.